I&EC research
Industrial & Engineering Chemistry Research

ARTICLE

pubs.acs.org/IECR

Characterization of Natural Zeolite Membranes for H_2/CO_2 Separations by Single Gas Permeation

S. A. Hosseinzadeh Hejazi, A. M. Avila, T. M. Kuznicki, A. Weizhu, and S. M. Kuznicki*

Department of Chemical and Materials Engineering, University of Alberta, Edmonton, AB, T6G 2 V4, Canada

ABSTRACT: Natural zeolite membranes can be used as a model for the development of robust molecular sieve membranes with superior separation characteristics. We describe the characterization of natural clinoptilolite membranes made from dense mineral deposits by single gas H_2 and CO_2 permeation. Permeability values as a function of temperature and pressure were analyzed on the basis of mass transport fundamentals of gas permeation through zeolite and nonzeolite pathways. H_2 and CO_2 fluxes through the membranes were fitted with a model based on a combination of zeolitic, Knudsen, and viscous transports so that the selective and nonselective flux fractions could be quantified. An increase in feed pressure increased the total permeance especially at low temperatures. The membranes were also characterized by XRD, SEM, and EDX analysis.

1. INTRODUCTION

Natural zeolite membranes which have been compacted by time and nature have recently been shown to demonstrate apparent molecular sieving of H_2 from H_2/CO_2 mixtures.[1] Such geomorphic sieve membranes are mechanically robust and with modification and development may increase the utility of molecular sieve membranes to many large scale separation processes. Because of the prolonged time and pressure that some natural zeolite deposits have experienced, intercrystalline grain boundaries, the primary weakness of synthetic zeolite membranes, have been fused or eliminated leaving materials with mechanical integrity unavailable in synthetic analogues.

Current environmental problems have created a need to search for cleaner fuels. Hydrogen has been proposed as a clean fuel because its combustion product is water. Unfortunately, hydrogen is not readily available in pure form. It can be obtained from steam reforming ($CH_4 + 2H_2O \rightarrow 4H_2 + CO_2$) and dry reforming ($CH_4 + CO_2 \rightarrow 2CO + 2H_2$).[2] After such reactions it must be separated from methane, carbon dioxide, and smaller amounts of other gases before it can be used as fuel.[3]

Current hydrogen separation membranes are made of palladium alloys or chemically and mechanically unstable organic polymer membranes.[4] Palladium membranes are costly, and can only be utilized at high temperatures.[4] Zeolite molecular sieves have uniform pore sizes which could make them promising for this separation. Zeolite membranes are capable of separating compounds by a combination of molecular sieving, selective adsorption, and differences in diffusion rates.[5−12] Synthetic molecular sieve membranes for hydrogen separation have also been studied intensively; however, their applications have been limited by both high production costs and lack of mechanical integrity including cracks or defects, and poor physical and chemical compatibility between the sieves and the supports on which they are grown.[13,14] While extensive research has been performed on the potential for hydrogen purification by synthetic molecular membranes,[15−17] very little attention has been paid to the natural zeolite-based membranes and their potential applications for purification.

Clinoptilolite is one of the most common of the natural zeolites. Clinoptilolite has a two-dimensional (2D) micropore/channel structure. The framework of clinoptilolite contains three sets of intersecting channels (A, B, C). The channels A and B are parallel to the *c*-axis and channels C are parallel to the *a*-axis. A channels are formed by strongly compressed 10-membered rings (aperture 4.4 × 7.6 Å), and the B channels are confined by 8-membered rings (aperture 4.7 × 4.1 Å). The C channels are also formed by eight-membered rings (aperture 5.5 × 4.0 Å).[18,19]

Clinoptilolite from the deposit at Castle Mountain (New South Wales, Australia) and from the deposit in Mount Kobau (British Columbia, Canada) are unusual. These materials have been compressed by their environments to the point where they have essentially no macroporosity. With bulk densities often approaching 2.5 g/cm^3, approximating the value expected for a single clinoptilolite crystal, these materials may in some ways be regarded as a solid crystalline zeolite block.

In this study we describe the characterization of disk-shaped natural clinoptilolite membranes by single H_2 and CO_2 permeation. H_2 and CO_2 fluxes through the membranes were obtained both experimentally and mathematically (by fitting with a model based on the combination of zeolitic, Knudsen, and viscous transports). Comparative parameters were introduced to characterize the membranes based on the relative average defect size, the cross sectional area of the nonzeolite pores, and the diffusion coefficients. This allowed for quantification of the selective flux fraction (zeolite and Knudsen fluxes) and nonselective flux fraction (viscous flux) for each analyzed membrane.

2. EXPERIMENTAL SECTION

2.1. Membrane Preparation. The natural zeolite rocks used in this study were from Mount Kobau, British Columbia, Canada, which is approximately located at N 49° 14′ 49″, W 119° 43′ 59″, and elevation of 1317 m. XRD analysis concluded that these

Received: March 16, 2011
Accepted: September 29, 2011
Revised: September 26, 2011
Published: September 29, 2011

dx.doi.org/10.1021/ie200529n | *Ind. Eng. Chem. Res.* 2011, 50, 12717–12726

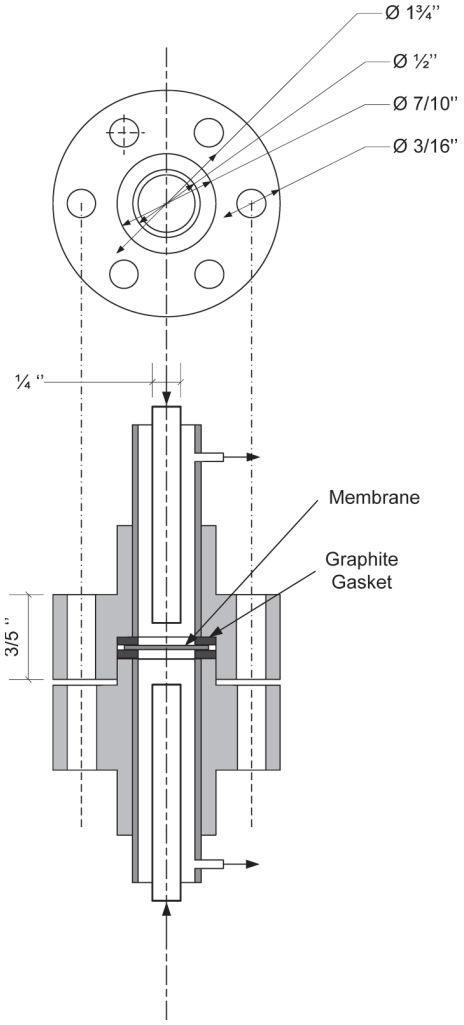

Figure 1. Schematics of the membrane testing system.

materials are rich in the natural zeolites/heulandite. Two thin discs (M1 and M2) were sectioned from a rock sample using a diamond saw with thicknesses of 2.2 mm and 2.1 mm each. A diamond polishing lap (180 mesh, Fac-Ette Manufacturing Inc.) was used to polish the discs which were then washed in an ultrasonic bath of deionized water for 30 min. Before each permeation test, the clean discs were dried in a temperature programmable oven as described by An et al.[1]

A JEOL 6301F field idem emission scanning electron microscope supplemented with energy dispersive X-ray spectroscopy (EDX) was used to examine the surface morphology of the membranes.

2.2. Adsorption Isotherms. CO_2 isotherms for the mineral zeolites composing the membranes were obtained by volumetric method on an Autosorb-1MP volumetric system (Quantachrome Instruments, Boynton Beach, FL) at temperatures of 298, 323, and 343 K and at pressures up to 100 kPa. The samples were activated at 573 K for 12 h under a vacuum of greater than 10^{-4} Torr before adsorption tests.

2.3. Gas Permeation Measurement. Gas permeation through the membranes was measured in a lab-made membrane testing system schematically shown in Figure 1.

The membranes were mounted into a stainless steel cell and sealed with graphite gaskets. The feed and permeate sides each had a stainless steel tube-shell configuration with an inlet gas flowing through the $^1/_4$ in. inside tube and an outlet gas flowing through the shell between the $^1/_4$ in. inside tube and $^1/_2$ in. outside tube. Argon (obtained from Praxair Canada, Inc.) was used as a sweep gas for the permeate side. The feed side pressure was controlled by a back pressure regulator and the permeate side was kept at ambient pressure. The flow rate of the feed side and the flow rate of the sweep gas (Ar) were kept at 100 mL/min (STP) and 200 mL/min (STP), respectively, throughout the measurements. The permeation system was placed into a tube furnace with a multipoint programmed temperature controller.

Single gas permeation of H_2 and CO_2 (obtained from Praxair Canada, Inc.) was measured at temperatures ranging from 298 to 573 K and feed pressures from 101.35 to 202.70 kPa. For the gas composition analysis, an online gas chromatograph (GC; Shimadzu GC-14B) with a HayeSep Q packed column and a thermal conductivity detector was used.

3. MODELING GAS TRANSPORT THROUGH THE MEMBRANES

Gas transport through a molecular sieve membrane is due to contributions from both zeolite and nonzeolite fluxes. Potential transport pathways are depicted in Figure 2.

3.1. Flow through Zeolite Pores. Gas transport through zeolite crystals is often referred to as surface diffusion, intracrystalline flux or zeolitic diffusion. The Maxwell−Stefan equation has been extensively used to describe the flux inside the zeolite crystal.[20] The flux of one component can be expressed as

$$N_{i,z} = -\rho q_s D_i T(\theta_i) \frac{\partial \theta_i}{\partial x} \quad (1)$$

The loading inside the zeolite (θ_i) is related to the partial pressure of component i by means of an adsorption isotherm model. If this model is a Langmuir type, then:

$$\theta_i = \frac{b_i P_i}{1 + b_i P_i} \quad (2)$$

and

$$T(\theta_i) = \frac{1}{1 - \theta_i} \quad (3)$$

The parameter b_i is dependent on temperature according to the Van't Hoff equation:

$$b_i = b_{i,0} \exp\left[\left(\frac{\Delta H_i}{R_g}\right)\left(\frac{1}{T_0} - \frac{1}{T}\right)\right] \quad (4)$$

where $b_{i,0}$ is the Langmuir adsorption constant at the reference temperature (T_0 = 298 K). With integration over x, the zeolitic flux can be expressed as

$$N_{i,z} = -\frac{\rho q_s D_i}{\Delta X} \ln\left(\frac{1 + b_i P_{\text{permeate}}}{1 + b_i P_{\text{feed}}}\right) \quad (5)$$

The diffusivity has an Arrhenius-type dependency with temperature:

$$D_i = D_{i,0} \exp\left[\left(\frac{E_i^D}{R_g}\right)\left(\frac{1}{T_0} - \frac{1}{T}\right)\right] \quad (6)$$

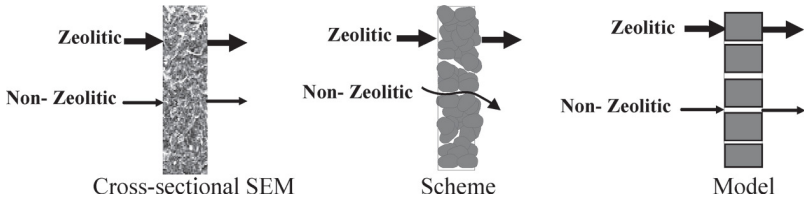

Figure 2. Outline of the gas transport pathways through the membrane.

where $D_{i,0}$ is the diffusivity of component i at the reference temperature (T_0 = 298 K) and E_i^D is the activation energy for diffusion.

At higher temperatures and lower pressures, adsorption isotherms often approach Henry's regime with adsorbed amounts that are linearly dependent on pressure:

$$q_i = K_i P_i \tag{7}$$

where K_i is the Henry's constant of component i. K_i is also dependent on temperature according to the Van't Hoff equation:

$$K_i = K_{i,0} \exp\left[\left(\frac{\Delta H_i}{R_g}\right)\left(\frac{1}{T_0} - \frac{1}{T}\right)\right] \tag{8}$$

Hence, zeolitic permeance can be expressed as

$$\Pi_{i,z} = \frac{\rho K_{i,0}}{\Delta X} D_{i,0} \exp\left[\left(\frac{E_i^D + \Delta H_i}{R_g}\right)\left(\frac{1}{T_0} - \frac{1}{T}\right)\right] \tag{9}$$

When $E_i^D + \Delta H_i > 0$, zeolitic permeance increases as temperature rises, at higher temperatures and lower pressures.

3.2. Flow through Nonzeolite Pores. Gas transport through nonzeolite pores are governed by Knudsen and viscous flux mechanisms. The Knudsen number (Kn), which is the ratio of the mean free path to the pore radius, indicates whether Knudsen diffusion or viscous flow dominates. For $Kn > 10$, transport is predominantly driven by Knudsen diffusion, and for $Kn < 0.01$, viscous flow dominates.[21] For Kn numbers between 0.01 and 10, both Knudsen diffusion and viscous flows contribute. In this study Knudsen numbers in a transitional regime between 0.5 and 1.0 were generally observed. The dusty-gas model[22] has been used to describe gas-phase transport in many different porous systems. This model, which describes mass transport in multicomponent systems, can be simplified for a single gas flow[23] as a linear combination of Knudsen and viscous contribution. The flux through nonzeolite pores can be expressed as

$$N_{i,nz} = N_{i,k} + N_{i,\nu} = \frac{1}{\tau}\frac{1}{\Delta X} D_{i,Kn} \frac{\Delta P_i}{R_g T} + \frac{1}{\tau}\frac{1}{\Delta X}\frac{r_i^2 P_m}{8\mu}\frac{\Delta P}{R_g T} \tag{10}$$

where the first and second terms represent Knudsen and viscous flows, respectively. $D_{i,Kn}$ is the Knudsen diffusivity of species i and is defined as

$$D_{i,Kn} = \frac{2}{3} r_i \sqrt{\frac{8000 R_g T}{\pi MW}} = 97 r_i \sqrt{\frac{T}{MW}} \tag{11}$$

It is also assumed that the dominant part of the nonzeolite gas transport occurs in free-transport pores of cylindrical shape with radii distributed around the mean value $\langle r_i \rangle$.[24]

Thus, total flux through the membrane can be estimated as

$$N_{i,t} = \propto N_{i,z} + (1 - \propto) N_{i,nz}, \quad \propto = \frac{Az}{At} \tag{12}$$

where $(1 - \propto)$ is the fraction of cross sectional area that corresponds to the defects or nonzeolite pores. The membrane permeance and ideal selectivities were estimated using the following expressions:

$$\Pi_i = \frac{N_{i,t}}{\Delta P_i} \tag{13}$$

$$S^i_{H_2/CO_2} = \frac{\Pi_{H_2}}{\Pi_{CO_2}} \tag{14}$$

4. RESULT AND DISCUSSION

4.1. Membrane Characterization. *Characterization Based on the Relative Average Pore Size.* The H_2 permeance at 298 K across the membrane can be considered as a combination of two permeance fractions. One fraction (Poiseuille or viscous contribution) is dependent on pressure while the other (Knudsen and zeolitic contributions) is not. The permeability of H_2 can be expressed as

$$\text{permeability} = \alpha_\nu [P^*] + \beta_{kz} \tag{15}$$

$$P^* = P_m \frac{\Delta P}{\Delta P_i} \tag{16}$$

The first term is pressure dependent while the second term is not. P_m is the mean pressure between the feed and the permeate stream. α_ν and β_{kz} are the slope and intercept of a linear fitting of the permeability data as a function of P^*; α_ν is a coefficient associated with viscous flow and β_{kz} is attributed to Knudsen and zeolite flow.

Based on eqs 5, 10, and 15, α_ν and β_{kz} are expressed as

$$\alpha_\nu = \frac{1}{\tau}\left(1 - \frac{A_z}{A_t}\right)\frac{\langle r_i^2 \rangle}{8\mu}\frac{1}{R_g T} \tag{17}$$

$$\beta_{kz} = \frac{1}{\tau}\left(1 - \frac{A_z}{A_t}\right) 97 \langle r_i \rangle \sqrt{\frac{T}{MW}}\frac{1}{R_g T} + \left[-\left(\frac{A_z}{A_t}\right)\frac{\rho q_s D_i}{\Delta P_i} \ln\left(\frac{1 + b_i P_{permeate}}{1 + b_i P_{feed}}\right)\right] \tag{18}$$

α_ν has a quadratic dependence on defect radii of the nonzeolite pores while β_{kz} is a linear function of defect radii.

The ratio α_ν/β_{kz} is a comparative parameter related to the medium pore size of different membranes. The membrane with

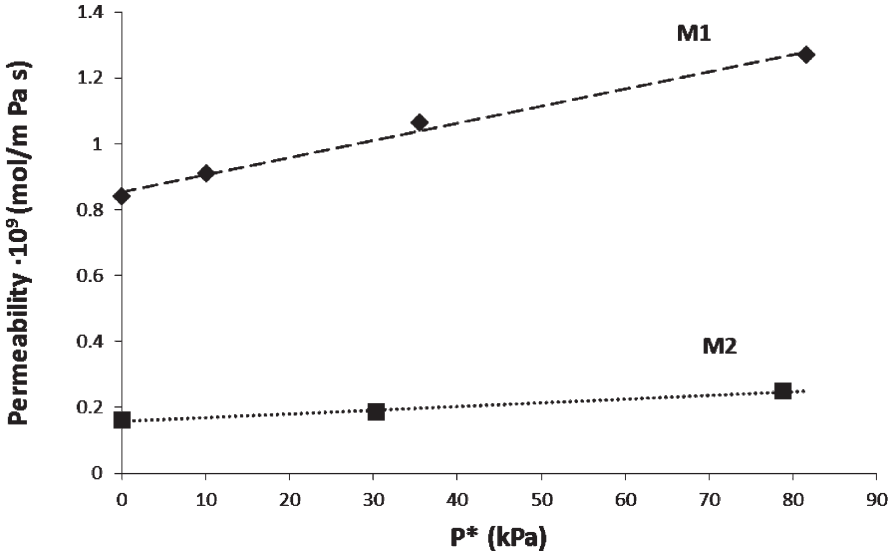

Figure 3. Permeability as a function of P^* at 298 K.

Table 1. Comparative Parameters for Membranes M1 and M2 at 298 K[a]

membrane/parameter	$a_1 \times 10^3$ (kPa^{-1})	$a_2 \times 10^3$ ($mol\ m^{-1}\ s^{-1}$)	$a_3 \times 10^3$ ($K^{0.5}$ Pa)	density ($kg\ m^{-3}$)
M1	6.10	14.0	5.0	1940
M2	7.09	2.2	3.3	2540

[a] $a_1 = \alpha_\nu/\beta_{kz}$; $a_2 = \beta_{kz}^2/\alpha_\nu$); $a_3 = \lambda/\omega$.

the smallest nonzeolite pore size corresponds to the lowest value of the α_ν/β_{kz} ratio. Lin and Burgraaf[25] studied the effect of pore size reduction on He permeability in alpha-alumina membranes. In their study, the total permeability was considered as a contribution of Knudsen and viscous flux. However, the total flux through the zeolite-based membranes includes the intrinsic zeolite flux in addition to the nonzeolite fluxes. It can be shown that α_ν/β_{kz} is a parameter of membrane defect size if $(\alpha_\nu/\beta_{kz})_{M2} > (\alpha_\nu/\beta_{kz})_{M1}$ and $(\alpha_\nu)_{M2} < (\alpha_\nu)_{M1}$ (Appendix A).

Figure 3 shows the permeability of each membrane as a function of P^*. M1 shows the highest permeability as the intersection at y-axis is the largest. The corresponding values of α_ν/β_{kz} for each membrane are listed in Table 1. M2 shows a slightly higher value for α_ν/β_{kz} ratio than M1. This is interpreted to mean that even though M1 has higher permeability, the average defect size is slightly larger for M2 than for M1. Figure 4 shows the effect of pressure on ideal selectivity for both membranes.

A comparison of relative average defect sizes (coefficient a_1 in Table 1) is consistent with the experimental values of the H_2/CO_2 ideal selectivities as the pressure increases at room temperature. Both H_2/CO_2 selectivities were higher than the corresponding Knudsen selectivity ($S^{Kn}_{H_2/CO_2} = (MW_{CO_2}/MW_{H_2})^{1/2} = 4.7$). H_2/CO_2 selectivity decreases as the feed pressure increases. The fraction of the "non-selective" viscous flux passing through the relatively larger nonzeolite pores increases as the total pressure difference rises. However, the selectivity of M2 decreases faster with pressure than the selectivity of M1. This is consistent with a larger defect size for M2 as compared to M1: $([\alpha_\nu/\beta_{kz}]_{M2} > [\alpha_\nu/\beta_{kz}]_{M1})$.

β_{kz}^2/α_ν is an additional parameter attributed to the nonzeolitic area of each membrane and the corresponding tortuosity (Appendix B).

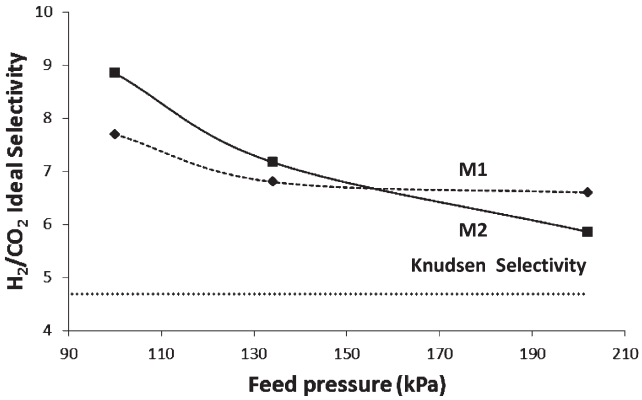

Figure 4. H_2/CO_2 ideal selectivity as a function of the feed pressure on the untreated natural zeolite membranes at 298 K.

The β_{kz}^2/α_ν values were calculated for the membranes listed in Table 1. It is worth noting that the membrane M1 has a significantly larger β_{kz}^2/α_ν coefficient than M2. M2 comes from a mineral sample with 30% higher density than M1. Thus, a lower β_{kz}^2/α_ν value for M2 can be associated with a higher density of its source rock. The higher density of the rock implies a smaller number of defects per membrane unit area. Membrane M2 has a lower defect area than M1 and a higher tortuosity.

A similar conclusion can be drawn from the results of single permeation experiments of H_2 at different temperatures. With no pressure difference between feed and permeate side, only zeolite and Knudsen flow contributions can be assumed.[26] The overall H_2 flux through the membrane can be expressed as

$$N_{i,t} = -\frac{A_z}{A_t}\frac{\rho q_s D_i}{\Delta X}\ln\left(\frac{1 + b_i P_{permeate}}{1 + b_i P_{feed}}\right) + \frac{1}{\tau}\left(1 - \frac{A_z}{A_t}\right)\frac{97}{\Delta X}\langle r_i\rangle\sqrt{\frac{T}{MW R_g T}}\Delta P_i \quad (19)$$

The first and the second term correspond to zeolite and Knudsen flow, respectively. Equation 19 can be simplified to

$$\text{permeability}\cdot\sqrt{T} = \omega\cdot C + \lambda \quad (20)$$

Table 2. Chemical Composition (Normalized wt %) of the Membrane Sample, Determined by Energy Dispersive X-ray Analysis

sample	M1	M2
Fe	3.25	8.24
Ca	6.02	7.04
Mg	0.78	1.76
Al	8.83	11.47
Si	47.95	45.55
K	2.88	2.88
Na	0.68	1.96
Cl	0	0
Ti	0.32	0.64
O	29.29	20.64

where ω and λ are the slope and intercept of a plot of "permeability $\cdot\sqrt{T}$" versus C, and ω, λ, and C can be expressed as

$$\omega = \frac{A_z}{A_t}\rho q_s D_{i,0} \tag{21}$$

$$\lambda = \frac{1}{\tau}\frac{A_i}{A_t}97\langle r_i\rangle\sqrt{\frac{1}{MWR_g}} \tag{22}$$

$$C = -\frac{\exp\left[\left(\frac{E_i^D}{R_g}\right)\left(\frac{1}{T_0}-\frac{1}{T}\right)\right]\sqrt{T}}{\Delta P_i}\ln\left(\frac{1+b_iP_{permeate}}{1+b_iP_{feed}}\right) \tag{23}$$

The ratio λ/ω is proportionate to the coefficient $1/\tau \cdot A_i/A_z \cdot \langle r_i\rangle$. Therefore, this ratio is related to both average defect size and fractional area of defects (nonzeolite pores).

Table 1 shows the corresponding values for the coefficient λ/ω for membranes M1 and M2. M2 has a smaller value of the coefficient $(1/\tau \cdot A_i/A_z \cdot \langle r_i\rangle)$ compared to M1. Previously, the comparison of values of β_{kz}/α_v for M1 and M2 (Table 1) reflected the fact that $\langle r_i\rangle$ is larger for M2. Therefore, the value of $(1/\tau \cdot A_i/A_z)$ for M2 should be much lower than M1, reflecting a smaller defect area and/or larger tortuosity for M2. This was also consistent with the permeability analysis at different pressures.

Profiles of permeability versus temperature can provide information on diffusion coefficients. The assessment of diffusivities in zeolite crystals is not a trivial issue.[27] However, the order of diffusivity can be estimated from the coefficient $\omega = (A_z/A_t)\,pq_sD_{H_2,0}$. Since A_z/A_t is a value approaching 1, and pq_s approaches ~200 mol/m^3 the order of magnitude of $D_{H_2,0}$ (diffusivity of H_2 through zeolite crystals at 298 K) can be estimated from the slope of the linear fitting of the plot of eq 20. $D_{H_2,0}$ is found to be on the order of 10^{-8} (m^2 s^{-1}), which is consistent with literature values for zeolite minerals with pore sizes similar to clinoptilolite. De Lara et al.[28] have reported diffusivity of H_2 to be equal to 3×10^{-8} (m^2 s^{-1}) in zeolite A at room temperature. In MFI membranes Sandström et al.[29] have obtained 3.6×10^{-8} (m^2 s^{-1}) for diffusivity of H_2 at room temperature.

The elemental surface analysis of each sample performed by EDX is shown in Table 2. M2 has a Si/Al ratio of ~4 which is lower than that of M1 (Si/Al ~5.5). Clinoptilolite generally has a Si/Al ratio between 4.2 and 5.3.[19] This higher value of Si/Al ratio for M1 could be associated with a larger amount of SiO_2 impurities

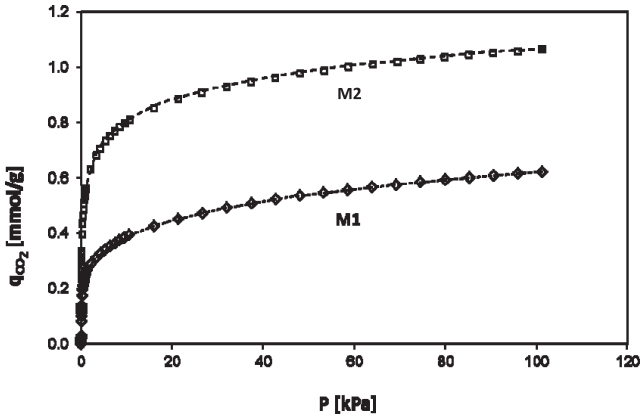

Figure 5. CO_2 isotherms for M1 and M2 at 298 K.

Table 3. Summary of M1 and M2 Membranes Characterization

Observation		Characteristic	M1	M2
Lower Si/Al ratio Higher CO_2 adsorption capacity	→	Higher zeolite content		✓
Higher selectivity at lower pressures Higher bulk density Lower permeability	→	Less non-zeolite area / Higher tortuosity		✓
Higher selectivity at higher Pressures	→	Smaller average defect size	✓	

and smaller zeolite content in this membrane. CO_2 isotherms measured for these materials (Figure 5) shows CO_2 adsorption capacity of M2 nearly twice as high as M1 at room temperature. This infers much higher clinoptilolite content in membrane M2 compared to M1. CO_2 molecules have strong interactions with most zeolite framework. Consequently, the CO_2 adsorption capacity (mol/kg) of the membrane material can be associated with its clinoptilolite content.[30]

M1 had higher permeability than M2 because the mass transport is less restricted due to the higher density of intercrystalline channels in the membrane. This is consistent with the lower zeolite content of M1 membrane compared to M2, and the lower bulk density of the original mineral sample. The key observations of the characterization of membranes M1 and M2 are summarized in Table 3.

4.2. Simulated Permeation Fluxes of Single Component H_2 and CO_2. Experimental data for H_2 and CO_2 permeances (at temperatures from 298 to 573 K and feed pressures from 101.3 to 202.7 kPa) were fitted with the model described in section 3. H_2 and CO_2 fluxes through the membrane can be expressed as a combination of zeolite, Knudsen, and viscous flux fractions. The adsorption enthalpy of CO_2 (ΔH_{CO_2}) on M2 was obtained from the adsorption isotherm data at different temperatures (Figure 6) using the Van't Hoff equation (eq 4) and was equal to −18 kJ/mol. The H_2 adsorption enthalpy ΔH_{H_2} and activation energies for diffusion of H_2 and CO_2 ($E_{H_2}^D$ and $E_{CO_2}^D$) were optimized estimated values from the fitting process. ΔH_{H_2} was estimated to be −3.0 kJ/mol and $E_{H_2}^D$ and $E_{CO_2}^D$ were calculated to be equal to 10.5 and 21.5 kJ/mol, respectively, based on this fitting process. Areán et al.[31] have reported a value of −3.5 kJ/mol for ΔH_{H_2} in FER zeolite, while Gu et al.[32] have obtained 18.1 kJ/mol for $E_{CO_2}^D$ in an MFI zeolite membrane. Kanezashi et al.[33] estimated a

value of 9.6 kJ/mol for $E^{D}_{H_2}$ through DDR zeolite membranes. The set of other model parameters is summarized in Table 4.

Effect of Temperature. Figures 7 and 8 show H_2 and CO_2 permeances as functions of temperature when both feed and permeate pressures are equal to 101.3 kPa. The driving force for permeation is associated with the partial pressure difference of either H_2 or CO_2. The H_2 or CO_2 fluxes through the membrane represent only a combination of zeolite and Knudsen contributions. Permeance associated with Knudsen diffusion decreases as the temperature rises.[34,35]

Permeance through membrane M2 slightly increased with temperature compared to M1 (Figures 7 and 8). The H_2 permeance for M2 increased ~25% when the temperature rose from 298 to 550 K. However, the permeance through M1 only increased ~5% in the same temperature range. This can be attributed to the larger contribution of zeolite flux to the total flux across M2 when the temperature rises. These results are consistent with the higher zeolite content of M2 and are further supported by CO_2 isotherms (section 4.1). CO_2 permeation shows similar behavior with an increase in temperature.

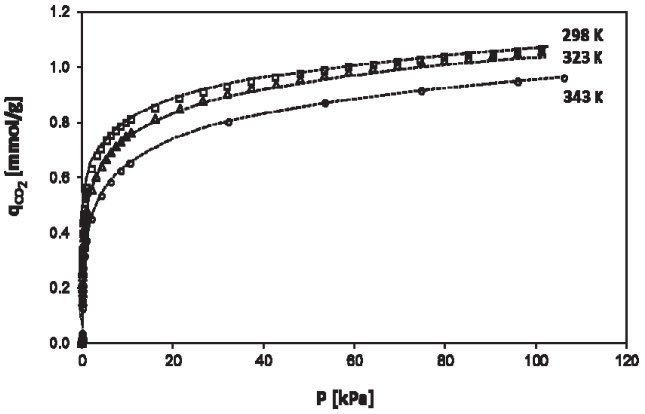

Figure 6. CO_2 isotherms for M2 at temperatures 298, 323, and 343 K.

Table 4. Values of the Model Parameters for Membrane M2

gas type/parameter	A (mol m^{-2} s)	B (mol K J^{-1})$^{0.5}$	C (mol K m J^{-1})
H_2	2.84×10^{-3}	1.62×10^{-6}	1.25×10^{-15}
CO_2	1.52×10^{-5}	8.67×10^{-7}	1.25×10^{-15}

Figure 9a shows H_2 permeance as a function of temperature for the M2 membrane at 34.5 kPa pressure drop. At these pressure conditions, in addition to the zeolitic and Knudsen fluxes, viscous transport also contributes to the total H_2 flux. Similar to Knudsen permeance, the permeance associated with viscous flux decreases with temperature. As the temperature increases, a higher fraction of H_2 total flux passes through the zeolite crystals. As shown in Figure 9b, the selective fraction of H_2 permeance able to provide separation selectivity (either molecular sieve or Knudsen), increases with temperature. On the contrary, the nonselective fraction related to the flux through relatively large nonzeolite pores (viscous flux) decreases with temperature. This membrane behavior can be advantageous for potential applications in the hydrogen separation industry where the process temperatures can reach higher than 523 K.[35]

Effect of Pressure. Simulated H_2 and CO_2 permeances as a function of temperature at different feed pressure values along with the experimental data, are shown in Figures 10 and 11. As both temperature and pressure increased, the mathematical model closely described the permeance behaviors for the membranes. The H_2 and CO_2 permeances through the membranes increased as the feed pressure rose. This is due to the higher viscous flux contribution through the relatively large nonzeolite pores. The permeance associated with the Knudsen flux remains constant as pressure increases. However, permeance related to the zeolitic flux is either constant or slightly decreases with pressure. CO_2 permeance is lower than H_2. The influence of pressure on the total permeance is slightly visible, at higher temperatures for both CO_2 and H_2. This can be explained by less viscous flux contribution as temperature rises. At higher temperatures, the zeolite flux and the Knudsen transport dominate (Figure 9b).

The optimized parameters A, B, and C for the permeation experiments through membrane M2 are defined as follows:

$$A = \propto \frac{\rho q_s D_{i,0}}{\Delta X} \tag{24}$$

$$B = \frac{1}{\tau}(1 - \propto)\frac{2}{3}\frac{\langle r_i \rangle}{\Delta X}\sqrt{\frac{8000}{\pi R_g}} \tag{25}$$

$$C = \frac{1}{\tau}(1 - \propto)\frac{1}{\Delta X}\frac{\langle r_i^2 \rangle}{8R_g} \tag{26}$$

The values of parameters A, B, and C are summarized in Table 4. The value of parameter A, related to the zeolite

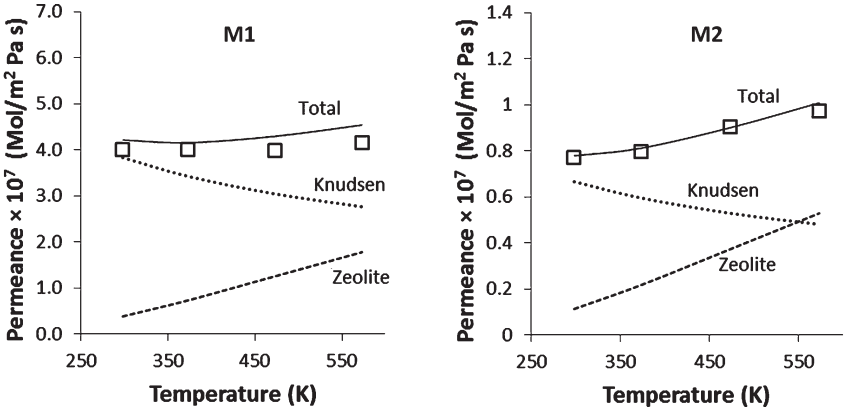

Figure 7. Contribution of the transport mechanisms to total H_2 permeance as a function of temperature across membranes M1 and M2. Feed and permeate pressures are equal to 101.3 kPa. The square represents experimental measurements.

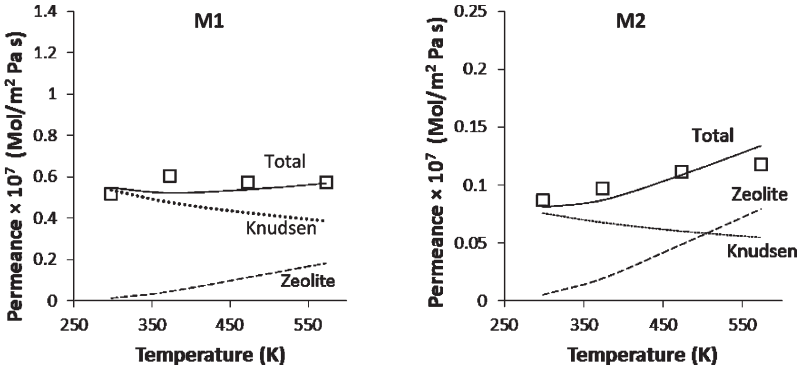

Figure 8. Contribution of the transport mechanisms to total CO_2 permeance as a function of temperature across M1 and M2. The square represents experimental measurements.

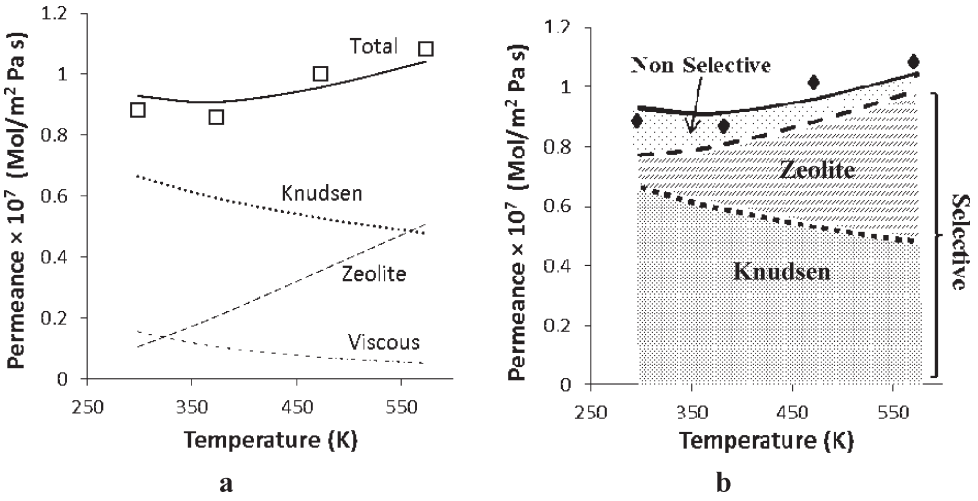

Figure 9. Dependence of H_2 permeance on temperature across M2. Contribution to total H_2 permeance from (a) different transport mechanisms and (b) selective and nonselective fractions at feed pressure of 135.8 kPa and permeate pressure of 101.3 kPa.

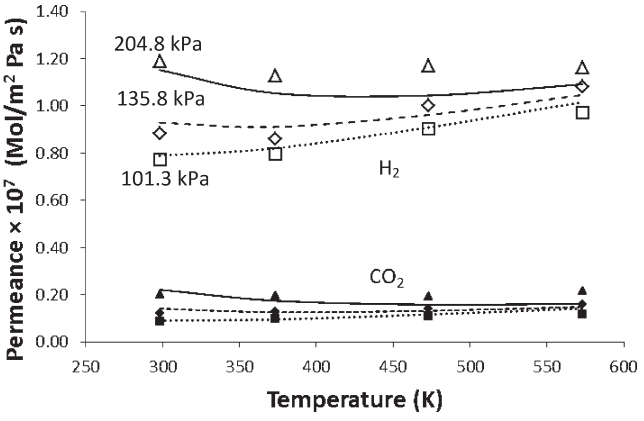

Figure 10. H_2 and CO_2 permeance for membrane M2 as a function of temperature at different feed pressures.

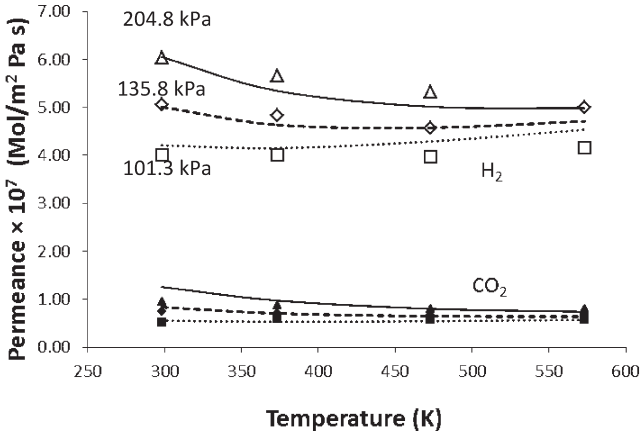

Figure 11. H_2 and CO_2 permeance for membrane M1 as a function of temperature at different feed pressures.

diffusion flux, is lower for CO_2 than for H_2. This is primarily associated with the lower diffusivity ($D_{i,0}$) of CO_2. The value of parameter B, associated with Knudsen diffusion is smaller for CO_2 than H_2. One explanation for this could be the possible reduction of Knudsen diffusivity as adsorption strength increases, as reported by Krishna et al.[36] The value of the parameter C (related to viscous flux) is the same for H_2 and CO_2 since it depends only on the membrane characteristics and not on the gas type.

CONCLUSIONS

Geomorphic natural zeolite membranes have shown promise in the separation for H_2 and CO_2 for the purification of H_2. H_2 and CO_2 permeation measurements through natural clinoptilolite based membranes were performed at temperatures ranging from 298 to 573 K, and feed pressures from 101.3 to 202.7 kPa. Membranes were characterized based on simple comparative parameters. The results from these analyses were consistent with the adsorption isotherms and experimental ideal permeance selectivities. A model based on the combination of zeolitic, Knudsen, and viscous transports was used to fit the H_2 and CO_2 permeance data. Temperature and pressure effects were studied in different membranes. A comparison of membranes from different mineral samples (M1 and M2) showed different zeolite flux contributions. Membrane M2, with a higher zeolite flux fraction, showed a lower permeability at room temperature than M1, but it had a steeper increase of H_2 permeance as temperature increased. Membrane M2 had higher bulk density and larger CO_2 adsorption capacity compared to M1. Total permeance increased with the increase of feed pressures especially at lower temperatures. The increase was less apparent at high temperatures. This is due to the larger contribution of the selective flux fractions (zeolite and Knudsen) compared to the nonselective flux fraction (viscous flux) at higher temperatures. This characterization technique can be advantageous in development and optimization of natural zeolite membranes for industrial applications, especially in high-temperature hydrogen separation industries.

APPENDIX A

It is possible to characterize a membrane's defect size by plotting permeability as a function of P^*, where $P^* = P_m(\Delta P/\Delta P_i)$, and

$$\text{permeability} = \alpha_\nu P^* + \beta_{kz} \tag{A-1}$$

where α_ν and β_{kz} are the slope and intercept of the best straight line fitting with permeability versus P^*.

For membranes having a defect size distribution, the permeation flux can be expressed as

$$N_{i,t} = \frac{A_z}{A_t} N_{i,z} + \frac{1}{\tau A_t} \int_{r_k > r_z}^{\infty} N_{i,nz}(r_k) a_i(r_k) n(r_k)\, dr_k \tag{A-2}$$

where $N_{i,nz}(r_k)$ is the permeation flux through a pore of radius r_k which is larger than the zeolite pore size ($r = r_z$); $a_i(r_k)$ is the cross-sectional area of each pore of radius r_k and $n(r_k)$ is the number pore size distribution which is related to the area pore size distribution, $\eta(r_k)$, through the following equation:[25]

$$\eta(r) = \frac{a_i(r_k) n(r_k)}{A_i} \tag{A-3}$$

Using eq A-3 in eq A-2, the permeation flux is

$$N_{i,t} = \frac{A_z}{A_t} N_{i,z} + \frac{1}{\tau}\left(1 - \frac{A_z}{A_t}\right) \int_{r_k > r_z}^{\infty} N_{i,nz}(r_k) \eta(r_k)\, dr_k \tag{A-4}$$

By using the corresponding equations for intracrystalline, Knudsen, and viscous transport mechanisms (eqs 5 and 10, respectively), the permeability can be expressed as:

$$\text{permeability} = \frac{N_{i,t}\Delta X}{\Delta P_i} = \alpha_\nu P^* + \beta_{kz} \tag{A-5}$$

where the parameters α_ν and β_{kz} are expressed as

$$\alpha_\nu = \frac{1}{\tau}\left(1 - \frac{A_z}{A_t}\right)\frac{\langle r_i^2\rangle}{8\mu}\frac{1}{R_g T} \tag{A-6}$$

$$\beta_{kz} = \underbrace{\frac{1}{\tau}\left(1 - \frac{A_z}{A_t}\right) 97 \langle r_i\rangle \sqrt{\frac{T}{Mw}}\frac{1}{R_g T}}_{\gamma} + \underbrace{\left[-\left(\frac{A_z}{A_t}\right)\frac{\rho q_s D_i}{\Delta P_i} \ln\left(\frac{1 + b_i P_{permeate}}{1 + b_i P_{feed}}\right)\right]}_{\Delta} \tag{A-7}$$

$\langle r_i\rangle = \int_{r_k > r_z}^{\infty} r_k\, \eta(r_k)\, dr_k$ is the integral mean of defect radii distribution and $\langle r_i^2\rangle = \int_{r_k > r_z}^{\infty} r_k^2\, \eta(r_k)\, dr_k$ is the integral mean of distribution of squared defect radii.

The terms γ and Δ in A-7 represent the permeabilities associated with Knudsen and zeolite flow, respectively. In this analysis it is shown that Δ is independent of pressure and membrane type. Because of the weak adsorption affinity of H_2, its zeolite flux is almost constant at 298 K for different feed pressures. Therefore, Δ can be assumed to be independent of pressure. A_z/A_t is a value that approaches 1, and its relative variation for different membranes is essentially negligible. As we use the same adsorption parameters for different rocks, Δ is also constant for different batches.

Thus, under these assumptions:

$$\left(\frac{\alpha_\nu}{\beta_{kz}}\right)_{M2} > \left(\frac{\alpha_\nu}{\beta_{kz}}\right)_{M1} \Rightarrow \left(\frac{\alpha_\nu}{\gamma + \Delta}\right)_{M2} > \left(\frac{\alpha_\nu}{\gamma + \Delta}\right)_{M1}$$

$$\Rightarrow (\alpha_\nu)_{M2}\gamma_{M1} + (\alpha_\nu)_{M2}\Delta > (\alpha_\nu)_{M1}\gamma_{M2} + (\alpha_\nu)_{M1}\Delta$$

If $(\alpha_\nu)_{M2} < (\alpha_\nu)_{M1}$ then $(\alpha_\nu)_{M2}\gamma_{M1} > (\alpha_\nu)_{M1}\gamma_{M2} \Rightarrow (\alpha_\nu/\gamma)_{M2} > (\alpha_\nu/\gamma)_{M1}$

$$\Rightarrow \left[\frac{\langle r_i^2\rangle}{\langle r_i\rangle}\right]_{M2}\frac{1}{97 \times 8\mu}\sqrt{\frac{MW}{T}} > \left[\frac{\langle r_i^2\rangle}{\langle r_i\rangle}\right]_{M1}\frac{1}{97 \times 8\mu}\sqrt{\frac{MW}{T}}$$

$$\Rightarrow \left[\frac{\langle r_i^2\rangle}{\langle r_i\rangle}\right]_{M2} > \left[\frac{\langle r_i^2\rangle}{\langle r_i\rangle}\right]_{M1} \Rightarrow (r_m)_{M2} > (r_m)_{M1}$$

where $r_m = \langle r_i^2\rangle/\langle r_i\rangle$ is defined as the flow averaged defect size.

Therefore, α_ν/β_{kz} is a parameter to characterize the membrane defect size.

In the case of uniform pore membranes: $\langle r_i\rangle = r_k$; $\langle r_i^2\rangle = r_k^2$; and $r_m = \langle r_i^2\rangle/\langle r_i\rangle = r_k$, then

$$\left(\frac{\alpha_\nu}{\gamma}\right)_{M2} > \left(\frac{\alpha_\nu}{\gamma}\right)_{M1} \Rightarrow (r_k)_{M2}\frac{1}{97 \times 8\mu}\sqrt{\frac{MW}{T}}$$

$$> (r_k)_{M1}\frac{1}{97 \times 8\mu}\sqrt{\frac{MW}{T}} \Rightarrow (r_k)_{M2} > (r_k)_{M1}$$

APPENDIX B

To characterize the membrane we plot permeability versus P^* (Appendix A). The linear function, its slope and intercept are defined by eqs A-1, A-6, and A-7, respectively. Ratio α_ν/β_{kz} can be used to characterize the membrane defect size. We introduce another parameter β_{kz}^2/α_ν that could also be very valuable in

characterization of uniform pore membranes. From eq A-7 it can be easily shown that

$$\beta^2 = \gamma^2 + \Delta^2 + 2\gamma\Delta \quad \text{(B-1)}$$

The second and third term of this expression can be neglected in comparison to γ^2 as zeolite flow (which is related to Δ) is negligible at 298 K. As a result, $\beta^2 = \gamma^2$ and

$$\frac{{\beta_{kz}}^2}{\alpha_v} = \frac{\gamma^2}{\alpha} = \frac{97^2\left(1-\frac{A_z}{A_t}\right)^2 {r_i}^2 \frac{T}{MW}\frac{1}{{R_g}^2 T^2}}{\left(1-\frac{A_z}{A_t}\right)\frac{{r_i}^2}{8\mu}\frac{1}{R_g T}}$$

$$= 97^2\left(1-\frac{A_z}{A_t}\right)\frac{8\mu}{R_g MW} \Rightarrow \frac{{\beta_{kz}}^2}{\alpha_v}$$

$$= \left(1-\frac{A_z}{A_t}\right)\varphi, \quad \varphi = 97^2\frac{8\mu}{R_g MW} \quad \text{(B-2)}$$

Thus, parameter ${\beta_{kz}}^2/\alpha_v$ characterizes the nonzeolitic area of membrane and is proportional to $(1 - (A_z/A_t))$.

AUTHOR INFORMATION

Corresponding Author

*E-mail: steve.kuznicki@ualberta.ca.

ACKNOWLEDGMENT

The authors thank Albana Zeko for assistance with manuscript development. Support from Canada Research Chair (Tier I) in Molecular Sieve Nanomaterials (S.M.K.), Alberta Water Research Institute (S.M.K.), and Helmholtz Alberta Initiative (S.M.K.) are gratefully acknowledged.

NOMENCLATURE

A_i = nonzeolite area of membrane surface (m^2)
A_t = Total area of membrane surface (m^2)
A_z = zeolite area of membrane surface (m^2)
b_i = Langmuir adsorption constant of component i (Pa^{-1})
$b_{i,0}$ = Langmuir adsorption constant of component i at (Pa^{-1})
D_i = diffusivity of component i ($m^2\ s^{-1}$)
$D_{i,0}$ = diffusivity of component i at zero loading ($m^2\ s^{-1}$)
$D_{i,kn}$ = Knudsen diffusivity of component i ($m^2\ s^{-1}$)
E_i^D = activation energy of component i (J mol^{-1})
K_i = Henry's constant of component i (mol kg^{-1} Pa^{-1})
$K_{i,0}$ = Henry's constant of component i at temperature T_0 (mol kg^{-1} Pa^{-1})
Kn = Knudsen number
MW = molecular weight (g mol^{-1})
$N_{i,k}$ = Knudsen flux (mol $m^{-2}\ s^{-1}$)
$N_{i,v}$ = viscous flux (mol $m^{-2}\ s^{-1}$)
$N_{i,z}$ = molar flux through zeolite pores (mol $m^{-2}\ s^{-1}$)
$N_{i,nz}$ = molar flux through nonzeolite pores (mol $m^{-2}\ s^{-1}$)
$N_{i,t}$ = total molar flux (mol $m^{-2}\ s^{-1}$)
P = pressure (Pa)
P_i = partial pressure of component i (Pa)
P_m = mean pressure (Pa)
q = adsorption capacity (mol kg^{-1})
q_s = saturation adsorption capacity (mol kg^{-1})
R_g = ideal gas constant (J $K^{-1}mol^{-1}$)
r_i = defect size (m)
$\langle r_i \rangle$ = integral mean of defect radii distribution (m)
$\langle r_i^2 \rangle$ = integral mean of distribution of squared defect radii (m^2)
r_k = defect size larger than r_i (m)
r_m = flow averaged defect size (m)
S^i = ideal selectivity
S^{kn} = Knudsen selectivity
T = temperature (K)
T_0 = reference temperature (K)
x = distance (m)

Greek Letters

α_v = coefficient defined by eq 17 (mol $m^{-1}\ s^{-1}\ Pa^{-2}$)
β_{kz} = coefficient defined by eq 18 (mol $m^{-1}\ s^{-1}$ Pa)
ΔH_i = enthalpy of adsorption of component i (J mol^{-1})
ΔX = membrane thickness (m)
θ = fractional loading
λ = coefficient defined by eq 20 (mol $K^{0.5}\ m^{-1}\ s^{-1}\ pa^{-1}$)
μ = viscosity (Pa s)
Π_i = membrane permeance of component i (mol $Pa^{-1}\ m^{-2}\ s^{-1}$)
$\Pi_{i,z}$ = zeolitic permeance of component i (mol $Pa^{-1}\ m^{-2}\ s^{-1}$)
ρ = density of zeolite (kg m^{-3})
ω = coefficient defined by eq 21 (mol $m^{-1}\ s^{-1}$)

REFERENCES

(1) An, W.; Swenson, P.; Wu, L.; Waller, T.; Ku, A.; Kuznicki, S. M. Selective separation of hydrogen from C1/C2 hydrocarbons and CO_2 through dense natural zeolite membranes. *J. Membr. Sci.* **2011**, *1−2*, 414–419.

(2) Nenoff. T. M. Defect-free thin film zeolite membranes for hydrogen separation and isolation, in: DOE/H_2. *Annu. Rev.Meet.* May 19, **2003**.

(3) Thomas, S.; Zalbowitz, M.; Cruz, J. *Fuel Cells—Green Power*; Los Alamos National Laboratory: Los Alamos, NM, 1999.

(4) Welk, M. E.; Nenoff, T. M.; Bonhomme, F. *Studies in Surfaces and Catalysis*; Elsevier B.V.: New York, 2004; Vol. 154.

(5) Xu, X.; Yang, W.; Liu, J.; Lin, L. Synthesis of NaA zeolite membrane by microwave heating. *Sep. Purif. Tech.* **2001**, *25*, 241–249.

(6) Coronas, J.; Falconer, J. L.; Noble, R. D. Characterisation and permeation properties of ZSM-five tubular membranes. *AIChE J.* **1997**, *43*, 1797.

(7) Yan, Y.; Davis, M. E.; Gavalas, G. R. Preparation of zeolite ZSM-5 membranes by in situ crystallization on porous-Al_2O_3. *Ind. Eng. Chem. Res.* **1995**, *34*, 1652.

(8) Coronas, J.; Santamaria, J. Separations using zeolite membranes. *Sep. Purif. Meth.* **1999**, *28*, 127.

(9) Van Bekkum, H.; Geus, E. R.; Kouwenhoven, H. W. Supported zeolite systems and applications. *Stud. Surf. Sci. Catal.* **1994**, *85*, 509.

(10) Kusakabe, K.; Kuroda, T.; Uchino, K.; Hasegawa, Y.; Morooka, S. Gas permeation properties of ionexchanged Faujasite-type zeolite membranes. *AIChE J.* **1999**, *45*, 1220.

(11) Aoki, K.; Kusakabe, K.; Morooka, S. Gas permeation properties of A-type zeolite membrane formed on porous substrate by hydrothermal synthesis. *J. Membr. Sci.* **1998**, *141*, 197.

(12) Burggraaf, A. J.; Vroon, Z. A. E. P.; Keizer, K.; Verweij, H. Permeation of single gases in thin zeolite MFI membranes. *J. Membr. Sci.* **1998**, *144*, 77.

(13) Gavalas, G. R. Zeolite Membranes for Gas and Liquid Separations. In *Materials Science of Membranes for Gas and Vapor Separation*; Yampolskii, Y., Pinnau, I., Freeman, B. D., Eds.; John Wiley & Sons, Ltd.: New York, 2006; pp 307−336.

(14) Caro, J.; Noack, M. Zeolite membranes—Recent developments and progress. *Microporous Mesoporous Mater.* **2008**, *115*, 215–233.

(15) White, J. C.; Dutta, P. K.; Shqau, K.; Verweij, H. Synthesis of ultrathin zeolite Y membranes and their application for separation of carbon dioxide and nitrogen gases. *Langmuir.* **2010**, *26*, 10287–10293.

(16) Tsapatsis, M.; Snyder, M. A. Hierarchical nanomanufacturing: From shaped zeolite nanoparticles to high-performance separation membranes. *Angew. Chem., Int. Ed.* **2007**, *46*, 7560–7573.
(17) Lin, Y. S.; Kumakiri, I.; Nair, B. N.; Alsyouri, H. Microporous inorganic membranes. *Separ. Purif. Method.* **2002**, *31*, 229–379.
(18) Ackley, M. W.; Giese, R. F.; Yang, R. T. Clinoptilolite: Untapped potential for kinetics gas separations. *Zeolites* **1992**, *12* (7), 780–788.
(19) Breck, D. W. *Zeolite Molecular Sieves—Structure, Chemistry, and Use*; John Wiley & Sons, Ltd: New York, 1974.
(20) Krishna, R.; Baur, R. Modelling issues in zeolite based separation processes. *Sep. Purif. Technol.* **2003**, *3*, 213–254.
(21) Colin, S. Rarefaction and compressibility effects on steady and transient gas flows in microchannels. *Microfluid. Nanofluid.* **2005**, *3*, 268–279.
(22) Mason, E. A.; Malinauskas, A. P. *Gas Transport in Porous Media: The Dusty-Gas Model*; Elsevier: Amsterdam, 1983.
(23) Thomas, S.; Schäfer, R.; Caro, J.; Seidel-Morgenstern, A. Investigation of mass transfer through inorganic membranes with several layers. *Catal. Today* **2001**, *1*−*3*, 205–216.
(24) Capek, P.; Hejtmánek, V.; Solcová, O. Permeation of gases in industrial porous catalysts. *Chem. Eng. J.* **2001**, *1*−*3*, 281–285.
(25) Lin, Y. S.; Burggraaf, A. J. Experimental studies on pore size change of porous ceramic membranes after modification. *J. Membr. Sci.* **1993**, *1*, 65–82.
(26) Cao, G. Z.; Meijernik, J.; Brinkman, H. W.; Burggraaf, A. J. Permporometry study on the size distribution of active pores in porous ceramic membranes. *J. Membr. Sci.* **1993**, *2*, 221–235.
(27) Kärger, J.; Caro, J.; Cool, P.; Coppens, M.; Jones, D.; Kapteijn, F.; Rodríguez-Reinoso, F.; Stöcker, M.; Theodorou, D.; Vansant, E. F.; Weitkamp, J. Benefit of microscopic diffusion measurement for the characterization of nanoporous materials. *Chem. Eng. Technol.* **2009**, *10*, 1494–1511.
(28) Cohen De Lara, E.; Kahn, R. Diffusivity of hydrogen and methane molecules in A zeolites: Neutron scattering measurements and comparison. *Zeolites* **1992**, *3*, 256–260.
(29) Sandström, L.; Lindmark, J.; Hedlund, J. Separation of methanol and ethanol from synthesis gas using MFI membranes. *J. Membr. Sci.* **2010**, *1*−*2*, 265–275.
(30) Sirkecioğlu, A.; Erdem-Şenatalar, A. Estimation of the zeolite contents of tuffaceous samples from the Bigadiç clinoptilolite deposit, Western Turkey. *Clay Clay Miner.* **1996**, *44* (5), 686–692.
(31) Areán, C. O.; Palomino, G. T.; Garrone, E.; Nachtigallová, D.; Nachtigall, P. Combined theoretical and FTIR spectroscopic studies on hydrogen adsorption on the zeolites Na-FER and K-FER. *J. Phys. Chem. B* **2006**, *1*, 395–402.
(32) Gu, X.; Tang, Z.; Dong, J. On-stream modification of MFI zeolite membranes for enhancing hydrogen separation at high temperature. *Microporous Mesoporous Mater.* **2008**, *1*−*3*, 441–448.
(33) Kanezashi, M.; Lin, Y. S. Gas permeation and diffusion characteristics of MFI-type zeolite membranes at high temperatures. *J. Phys. Chem. C* **2009**, *9*, 3767–3774.
(34) Tarditi, A. M.; Lombardo, E. A.; Avila, A. M. Xylene permeation transport through composite Ba-ZSM-5/SS tubular membranes: Modeling the steady-state permeation. *Ind. Eng. Chem. Res.* **2008**, *7*, 2377–2385.
(35) Ritter, J. A.; Ebner, A. D. State-of-the-art adsorption and membrane separation processes for hydrogen production in the chemical and petrochemical industries. *Sep. Sci. Technol.* **2007**, *6*, 1123–1193.
(36) Krishna, R. Describing the diffusion of guest molecules inside porous structures. *J. Phys. Chem. C* **2009**, *46*, 19756–19781.